

# Field Testing of Feedforward Collective Pitch Control on the CART2 Using a Nacelle-Based Lidar Scanner

David Schlipf<sup>1</sup>, Paul Fleming<sup>2</sup>, Florian Haizmann<sup>1</sup>, Andrew K. Scholbrock<sup>2</sup>, Martin Hofsäß<sup>1</sup>, Alan Wright<sup>2</sup> and Po Wen Cheng<sup>1</sup>

<sup>1</sup> Stuttgart Wind Energy Research (SWE), Universität Stuttgart, Germany,

<sup>2</sup> National Renewable Energy Laboratory (NREL), USA

E-mail:

<sup>1</sup> David.Schlipf/Florian.Haizmann/Martin.Hofsass/PoWen.Cheng@ifb.uni-stuttgart.de

<sup>2</sup> Paul.Fleming/Andrew.Scholbrock/Alan.Wright@nrel.gov

**Abstract.** This work presents the first results from a field test to prove the concept of LIDAR assisted collective pitch control using a scanning LIDAR device installed on the nacelle of a research turbine. The purpose of the campaign was to show that a reduction of rotor speed variation is feasible with a feedforward update without changing the feedback controller. Although only a small amount of data could be collected, positive effects can be observed not only on the rotor speed but also on tower, blade and shaft loads in the case that the correlation of the wind preview and the turbine reaction is taken into account.

## 1. Introduction

LIDAR (LIght Detection And Ranging) systems are able to provide information about the wind field approaching a wind turbine in advance, which can be used to assist wind turbine control. While early work on LIDAR-assisted control was made by [1], this field of investigations has increased significantly in recent years, and several feedforward and model predictive controllers have been proposed for load reduction or increasing the energy yield, see e.g., [2]-[7]. The feedforward collective pitch control as proposed in [8] has the advantage, that it can be implemented as a simple update to existing feedback controllers. The core of this controller is an adaptive filter, which accounts for the changing correlation and mean wind speed. This work presents the first results from a field test to prove the concept, using a scanning LIDAR device installed on the nacelle of the CART2 (Controls Advanced Research Turbine, 2-Bladed, [9]) turbine at NREL.

This paper is organized as follows. Section 2 summarizes the experimental environment. In Section 3 the LIDAR sensing process and the used controller are outlined. The correlation of the LIDAR and the turbine is described in Section 4. Section 5 presents the measured results, and conclusions and future work are discussed in Section 6.

## 2. Test Environment

In this section the test site, turbine and LIDAR system for the field testing are described.

### 2.1. The Test Site

The field testing took place at the National Wind Technology Center (NWTC) in Boulder, Colorado, which is part of the National Renewable Energy Laboratory (NREL). Due to its location directly in front of the Rocky Mountains Front Range NWTC offers good conditions during the wind season in winter to perform any kind of field test. Since the wind conditions are rather gusty and extreme, especially tests under extreme conditions can be performed there.

### 2.2. The Test Turbine

Among several multi-megawatt turbines, the NWTC owns two mid-sized turbines, which are dedicated to the testing of new and advanced control algorithms of wind turbines, the so-called Controls Advanced Research Turbines (CARTs). These two turbines are two 600 kW Westinghouse *WTG-600* turbines, which were originally deployed in a wind farm on Hawaii. The CART2 (Figure 1a) is still equipped with the original two-bladed rotor, but was retrofitted with high-speed electromechanical pitch drives, a new fully controllable power electronics, and is heavily instrumented with strain gauges, accelerometers, as well as a dedicated meteorological tower, installed 80 m in front of the turbine in mean wind direction ( $292^\circ$ ). The turbine has a rotor diameter of  $D = 42.7$  m at a hub height of 36.9 m and runs at a rated rotor speed of 41.7 rpm. Since it is a two-bladed turbine, it has a teetered hub, which was free during the test runs. Furthermore, a control system was developed and implemented in LabVIEW by NWTC engineers. This control system runs as a 400 Hz real-time system, which needs to be supervised by an engineer. Although, it handles all possible operating failures, an unattended run of this test turbine is not yet possible. However, it offers engineers an easy way of implementing their own controller code as a DLL, which is then loaded by the LabVIEW framework control system. For this work the DLL was created as an export from MATLAB/Simulink code.

### 2.3. The Used LIDAR System

A scanning LIDAR system from the University of Stuttgart was installed on the CART2 in early 2012. It was placed on a frame which was mounted on the front top of the railing of the platform on top of the CART2's nacelle, as it can be seen in Figure 1b. To compensate the  $3.77^\circ$  tilt of the CART2 nacelle, the LIDAR was mounted with a counter angle of about  $3.7^\circ$ , so that the system itself is horizontal aligned.

The system consists of two parts: A Windcube V1 from *Leosphere* and a scanner unit developed at the University of Stuttgart [10]. Since the original Windcube was designed for site assessment with its beam pointing upwards, a two-degrees-of-freedom mirror for redirecting the beam in any position within the mirror's range was installed in a second casing, which allows pointing sideways. Figure 1c shows a picture of the scanner's mirror and the side window through which the laser beam emits. A modified software synchronizes the laser with the two motor stages. This software allows in principle a free design of the scanning trajectories within the mechanical constrains, but in this campaign only two different scanning modes were used: In the "StartStop" mode (see Figure 2a) the center of the acquisition time  $T_{ACQ}$  is centered between two stop times  $T_{XPS}$ . In the "BangBang" mode (see Figure 2b) the center of the acquisition time  $T_{ACQ}$  coincides with one stop time  $T_{XPS}$  to be faster than the "StartStop" mode but to distribute the measurement over a small angle  $\alpha$ . The LIDAR raw data are the line-of-sight wind speed  $v_{los}$ , the Carrier to Noise Ratio (CNR), the two angular positions of the motors, the focus length along the beam for each focus distance and the times  $T_{ACQ}$  and  $T_{XPS}$ . The modified software allows to use up to 5 scan distances (see Figure 2c).



(a) The CART2.

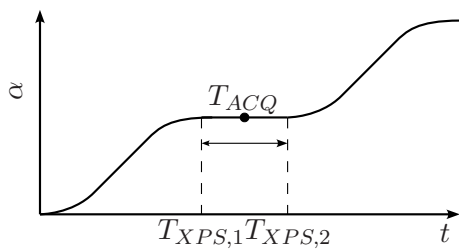


(b) The SWE-LIDAR installed on the CART2.

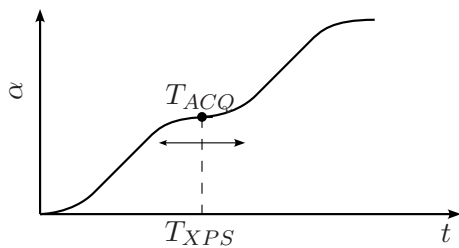


(c) Two-DOF mirror seen from internal webcam.

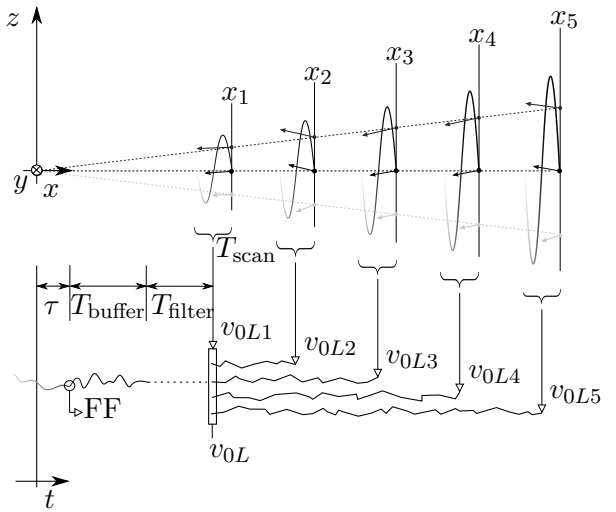
**Figure 1.** Test environment at NREL.



(a) Scan mode StartStop.



(b) Scan mode BangBang.



(c) Scope of the wind prediction.

**Figure 2.** Scan of the wind inflow.

### 3. Controller Design

This section gives a short overview of the reconstruction of the rotor effective wind speed from the LIDAR data and the feedback and feedforward controller. Implementation issues are also addressed.

#### 3.1. The Feedback Controller

The baseline feedback controller is a slightly modified standard wind turbine controller. The torque controller uses a normal  $k\Omega_g^2$  law in region 2 and a constant torque is applied in region 3. The pitch controller is called a PI/ID type controller, which is a PI controller with an additional integrated derivative term. The design and motivation for this control law are provided in [11]. In practice, the controller performs similarly to a normal PI controller. Both the torque and pitch controller follow the standard practice of feeding back only the generator speed term for control. The controller includes several additional elements including roll-off filters, notch filters on certain resonance and disturbance frequencies, and finally a tower-resonance avoidance scheme. The baseline controller is used as a reference in a number of past studies. For example, it is used as the base controller with which to compare a state-space IPC controller in [12].

#### 3.2. The LIDAR Preview

For this campaign circular trajectories, with 6 focus points in 5 focus distances equally distributed between  $x_1 = 1D = 42.7$  m and  $x_5 = 2D = 85.3$  m (see Figure 2c) were used. The duration of one scan is for the ‘‘BangBang’’ mode  $T_{Scan} = 1.33$  s and for the ‘‘StartStop’’ mode  $T_{Scan} = 2.42$  s. For the acquisition of one measurement 2000 pulses with an average duration of 0.144 s are used. For each distance  $j$ , data points with bad synchronization or low CNR (see Section 4) are removed. For the remaining data points the longitudinal wind component is reconstructed assuming lateral and vertical wind components to be zero and by averaging over the last trajectory

$$v_{0Lj}(t) = \frac{1}{6} \sum_{i=1}^6 v_{los,ij}/l_{xi}, \quad (1)$$

where  $l_{xi}$  is the laser vector component in inflow wind direction. The obtained time series  $v_{0Lj}$  is time-shifted according to Taylor’s frozen turbulence hypothesis (see Figure 2c), which assumes that the turbulent wind field moves with the average wind speed: The time to reach the first focus distance is assumed to be  $(x_j - x_1)/\bar{v}$ , where  $\bar{v}$  is the mean wind speed. The LIDAR estimate of the rotor effective wind speed  $v_{0L}(t)$  is then calculated by

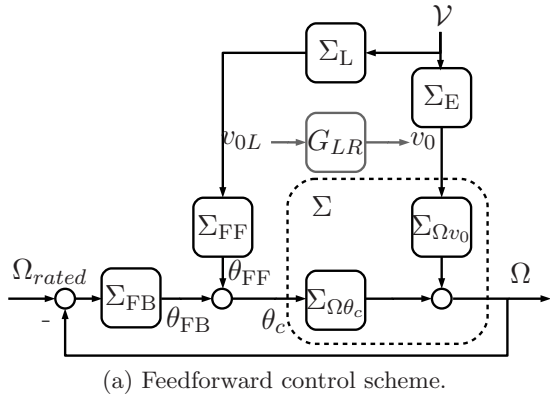
$$v_{0L}(t) = \frac{1}{5} \sum_{j=1}^5 v_{0Lj}(t - (x_j - x_1)/\bar{v}). \quad (2)$$

The wind speed preview  $v_{0L}$  is filtered by a low-pass filter, and the time delay introduced by the filter has to be considered as explained in the next subsection.

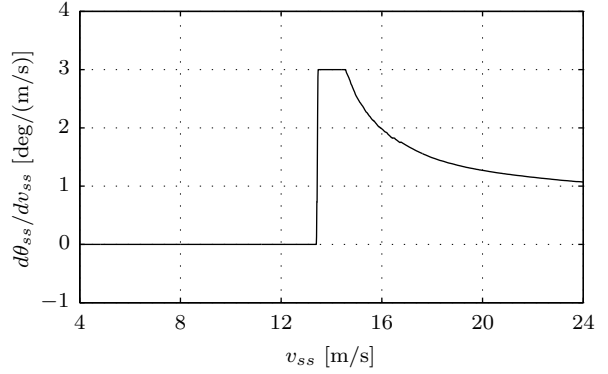
#### 3.3. The Feedforward Controller

The feedforward controller (see Figure 3a) is based on the work in [8] and combines the baseline feedback controller with a feedforward pitch rate update. The main control goal of the collective pitch feedback controller  $\Sigma_{FB}$  is to maintain the rated rotor speed  $\Omega_{rated}$  by adjusting the demanded pitch angle  $\theta_c$ . A wind field  $\mathcal{V}$  evolves to  $v_0$  on its way to the turbine and disturbs the system  $\Sigma$ . The measurement of the wind field in front of the turbine by a LIDAR system  $\Sigma_L$  yields  $v_{0L}$ . The disturbance could be perfectly compensated by a feedforward controller

$$\Sigma_{FF} = -\Sigma_{\Omega\theta_c}^{-1} \Sigma_{\Omega v_0} \Sigma_E \Sigma_L^{-1}, \quad (3)$$



(a) Feedforward control scheme.



(b) Static pitch rate curve of the CART2.

**Figure 3.** The feedforward controller.

if the complete system was known and  $\Sigma_{\Omega\theta_c}$  as well as  $\Sigma_L$  were invertible. Due to its complexity, the inversion of  $\Sigma_{\Omega\theta_c}$  cannot be found for an aeroelastic model. Here, the stationary pitch curve  $\theta_{ss}(v_{ss})$  is used to substitute  $-\Sigma_{\Omega\theta_c}^{-1} \Sigma_{\Omega v_0}$ . For real applications, it is beneficial to use a pitch rate update  $\dot{\theta}_{FF}$  instead of  $\theta_{FF}$ :

$$\dot{\theta}_{FF} = \dot{v}_0 \frac{d\theta_{ss}}{dv_{ss}}(v_0). \quad (4)$$

Figure 3b shows the air density corrected static pitch rate curve  $d\theta_{ss}/dv_{ss}$  for the CART2, limited to 3 deg/(m/s), to avoid high pitch rate near the rated wind speed (see [8]).

Further simplifications have to be made for  $\Sigma_E \Sigma_L^{-1}$ , because information is lost by the LIDAR measurement due to the spacial averaging and thus  $\Sigma_L$  cannot be inverted. Also  $\Sigma_E$  is quite complex to model. However, the transfer function  $G_{LR}$  from the LIDAR estimate of the wind speed to the rotor effective wind speed can be estimated from measured data via the auto correlation spectrum of the measured wind speed  $S_{LL}$  and the cross correlation spectrum  $S_{SL}$  between the measured and the rotor effective wind speed. Due to its low pass behavior and the preview provided by the LIDAR, the transfer function is approximated by a second-order Butterworth filter  $G_{filter}$  and a time delay:

$$G_{LR} = \frac{S_{LR}}{S_{LL}} \approx G_{filter}(s) e^{T_{buffer}s}. \quad (5)$$

The filter is parametrized by a static gain  $G_0$  and a cut-off frequency  $f_{cutoff} = \hat{k}\bar{v}/(2\pi)$ , where  $\hat{k}$  is the maximum coherent wavenumber. The time delay is obtained from the following considerations: With Taylor's hypothesis, the wind needs the time  $x_1/\bar{v}_1$  to evolve from the first focus distance to the turbine. Due to the averaging over the full trajectory,  $v_{0L}$  is already delayed by  $T_{scan}/2$ . The filter delay is approximated by  $T_{filter}$ . For using the filtered wind in the feedforward controller (4) instead of  $v_0$ , the signal has to be synchronized with  $v_0$  reaching the rotor plane. Therefore the necessary time delay is

$$T_{buffer} = \frac{x_1}{\bar{v}} - \frac{1}{2}T_{scan} - T_{filter} - \tau. \quad (6)$$

The time  $\tau$  can be used to compensates for the slow down of the wind due to the higher pressure in front of the turbine or small errors in the model reduction (see [3]).

#### 4. Correlation Study

Before applying the LIDAR feedforward update to the CART2, a correlation study has been made to determine the maximum coherent wavenumber for the filter design and to adjust  $\tau$ . Therefore, the measured rotor effective wind speed  $v_{0L}$  from the LIDAR is compared to an estimate from turbine data. The correlation study was used to detect problems with hard targets.

##### 4.1. The Estimator for the Rotor Effective Wind Speed

The rotor effective wind speed  $v_0$  is obtained from simulated turbine data by an estimator similar to the one presented in [13]. Here, the CART2 is modeled by

$$J\dot{\Omega} + M_{LSS} = M_a, \quad (7)$$

where  $M_a$  is the aerodynamic torque,  $M_{LSS}$  is the low-speed shaft torque, and  $J$  is the overall sum of the moments of inertia about the rotation axis.

Moreover, the aerodynamic torque acting on the rotor with radius  $R$  is:

$$M_a = \frac{1}{2}\rho\pi R^3 \frac{c_P(\lambda, \theta)}{\lambda} v_0^2 \quad (8)$$

where  $\rho$  is the air density,  $\lambda$  is the tip-speed ratio

$$\lambda = \frac{\Omega R}{v_0}, \quad (9)$$

and  $c_P$  is the effective power coefficient, obtained from steady-state simulation [14].

With measured data of  $\Omega$  and  $M_{LSS}$  the aerodynamic torque  $M_a$  can be calculated using (7). Due to numerical issues (8) is reorganized in a cubic equation in  $\lambda$ :

$$\lambda^3 = \frac{1}{2}\rho\pi R^5 \frac{c_P(\lambda, \theta)}{M_a} \Omega^2. \quad (10)$$

Because of the  $\lambda$ -dependency of  $c_P$ , an explicit expression cannot be found. The equation is solved with a set of  $M_a$ ,  $\Omega$  and  $\theta$ , and a three-dimensional look-up table  $v_0(M_a, \Omega, \theta)$  is generated, which can then be used to get a time series of  $v_0$  by a three-dimensional interpolation.

##### 4.2. The Hard Target Problem

When first comparing the LIDAR estimate  $v_{0L}$  running the ‘‘BangBang’’ scanning mode with the turbine estimate  $v_0$ , lower values were discovered. A detailed investigation of the data revealed values of  $v_{los}$  around 0 m/s, typical for an impact with a hard target. It is assumed due to the position in the trajectory (see Figure 4b) and the yaw dependency, that the met mast and the guy wires are responsible. Figure 4a shows exemplary the  $v_{los}$  data distribution over the CNR of a 10 min raw data file. Impact with the rotating blades can easily identified by a lower CNR limit, depending on the trajectory, the number of averaged shoots, and the aerosol concentration. Here  $-18$  dB was used. This cannot be done for the hard target issue, because the CNR value are distributed along the CNR range of the normally reliable data. Due to the high occurrence of this issue, using only data with high  $v_{los}$  was not considered. Instead, two strategies were used:

- (i) Use the ‘‘StartStop’’ mode and remove all data online with a CNR value above  $-5$  dB, because it was assumed that with this modification the probability of an impact can be minimized and the CNR will be maximized in the case of an impact. This implies that the correlation is supposed to be lower due to the slower trajectory.
- (ii) Cut off the FFT spectra at bin 15. The peak detection algorithm is than able to find the second minor peak, see 4c. This implies that  $v_{los}$  below 6 m/s cannot be detected.

The second approach gave better results as can be seen in the following section.

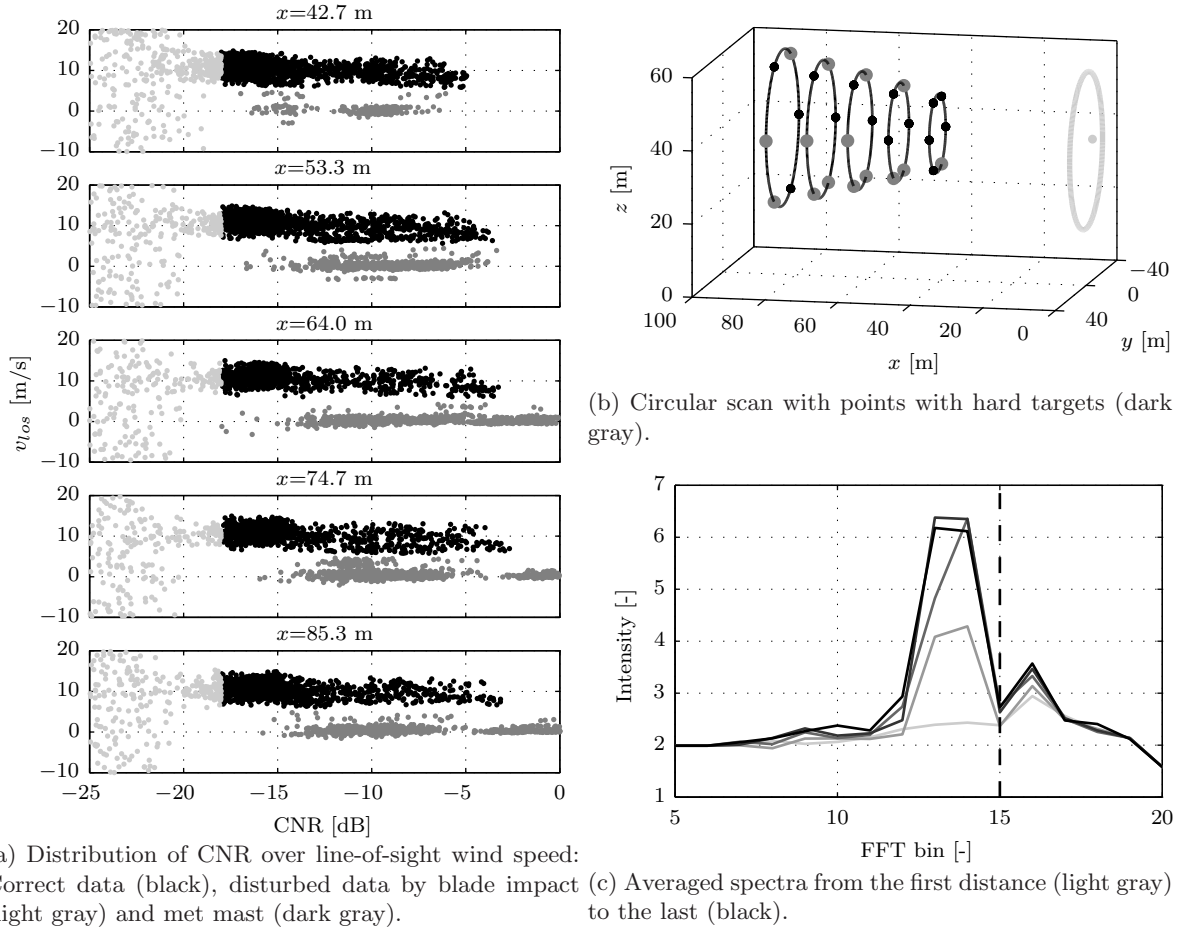


**Figure 4.** The hard target problem.

**Table 1.** Overview of evaluated data.

Block ID	Start Time	End Time	FFoff-Section	FFon-Section		$\hat{k}$ [rad/m]	Yaw [deg]	Scan mode
				good	bad			
1	04-13 15:39:29	04-13 16:34:29	8	0	0	-	307	-
2	05-17 01:18:28	05-17 01:28:28	0	0	6	0.02	296	StartStop
3	06-05 23:20:59	06-05 23:30:59	0	6	0	0.06	148	BangBang
4	07-25 04:11:12	07-25 04:16:11	5	3	0	0.06	250	BangBang

#### 4.3. Design of the Filter

Due to problems with the data acquisition system of the turbine and the low wind season, only 4 blocks of significant data were collected during the campaign (see Table 1). The data blocks are divided in sections with the feedforward controller on with high and low correlation (FFon good/bad) and sections with only the feedback controller (FFoff). In the case of Block 2 the hard target issue could not be reduced by the StartStop scan mode.

Figure 5 shows the two rotor effective wind speed estimates of Block 4. A high correlation can be detected for the whole period before the emergency stop due to a data acquisition problem. The LIDAR signal has a similar preview time over the whole data set, but at  $t \approx 300$  s the LIDAR detects the gust with a higher preview. This is more obvious in the cross correlation plot in Figure 6: For most of the time of Block 4 and also for Block 3 with  $\tau = -0.6$  s the time

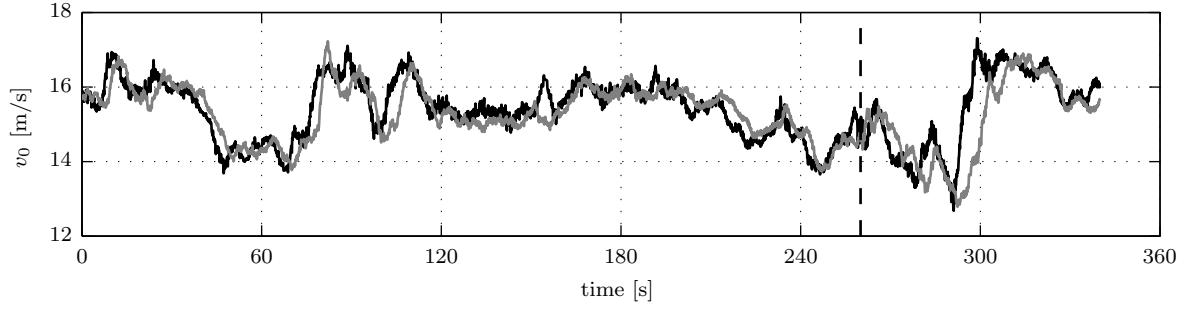


**Figure 5.** Rotor effective wind speed estimates from the turbine (gray) and the LIDAR (black).

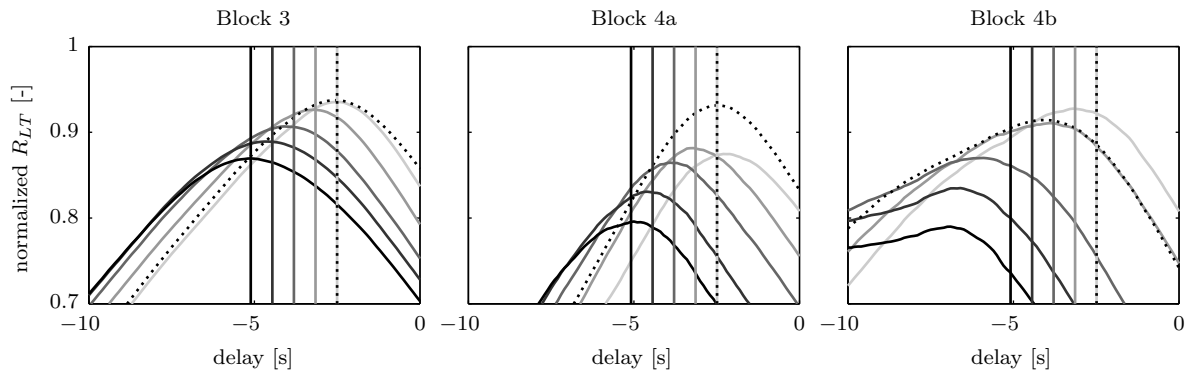


**Figure 6.** Cross correlation between the turbine and LIDAR: the first distance (light gray) to the last (black) and the average  $v_{0L}$  (dotted). The lines indicate the predicted preview.

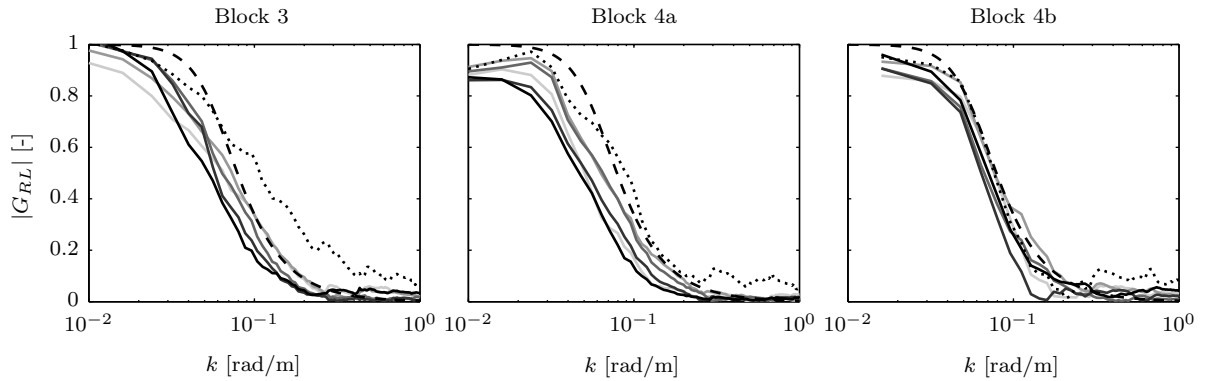


**Figure 7.** Transfer function between the turbine and the first distance (light gray) to the last (black) and compared to the average  $v_{0L}$  (dotted). The dashed line shows to used filter.

shift of each distance is close to the time shift according to Taylor's hypothesis.

Figure 7 depicts the measured transfer function between the  $v_0$  and  $v_{0L}$  as well as the chosen filter. The static gain is set to  $G_0 = 1$  and the maximum coherent wavenumber as a compromise to  $k = 0.06$  rad/m. The average wind speed  $\bar{v}$  is calculated by a moving average over 180 s. Further studies are necessary to investigate, if the problem detected in Figure 5 can be improved by a shorter average time. The integral time scale may be a good approach.

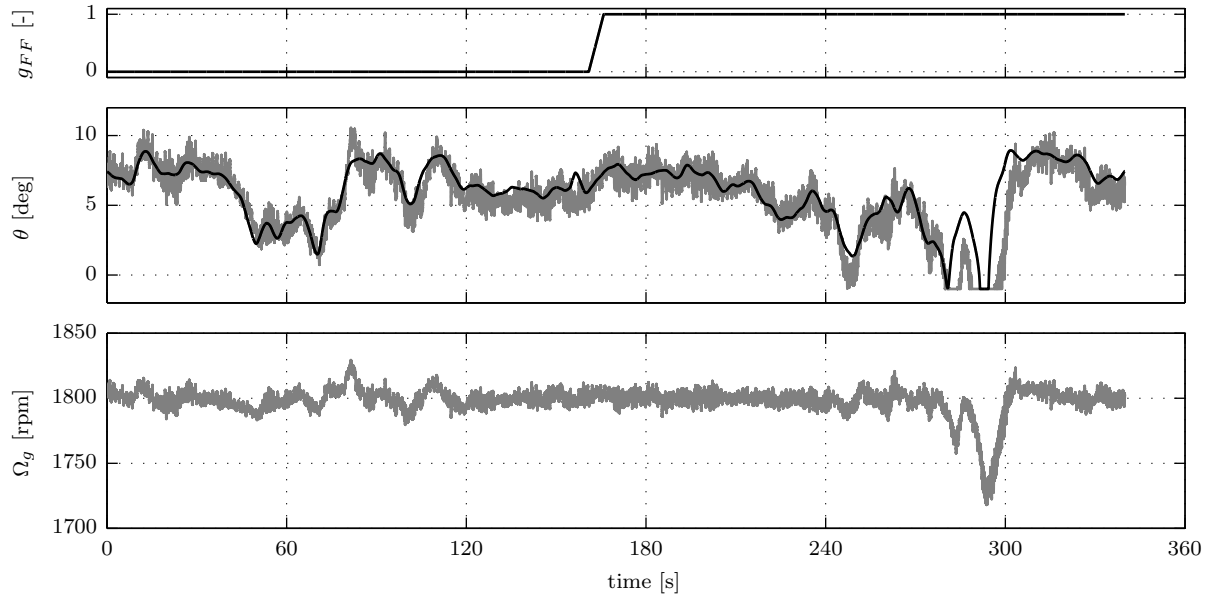


**Figure 8.** FF switch, the measured pitch angle (gray) and the feedforward pitch angle (black) and the generator speed for Block 4.

## 5. Results

Although the collected data yields only a limited evaluable amount of data so far, the shown results are considered to be indicative because the wind conditions of the evaluated blocks are comparable. As shown in Figure 9a, the turbulence intensities of the evaluated blocks are distributed similarly.

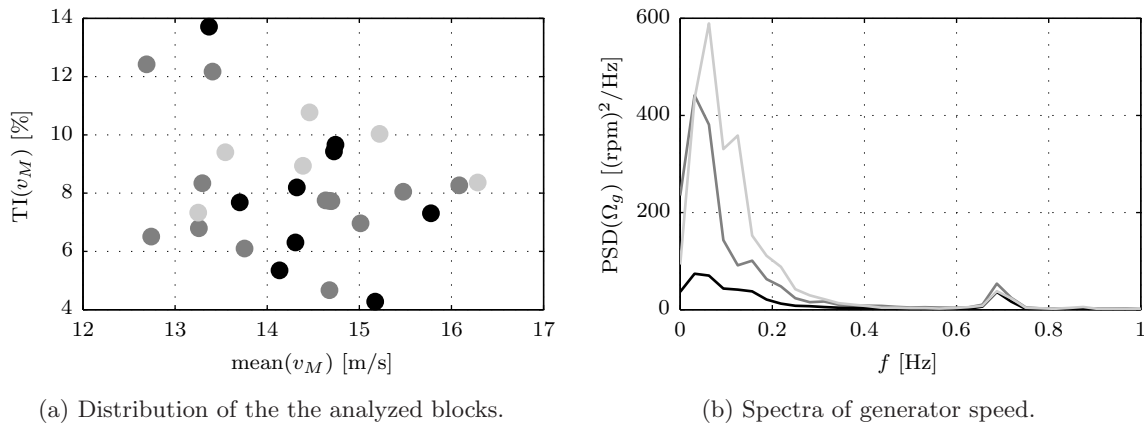
Figure 8 shows the smooth enabling of the feedforward controller by changing the FF switch  $g_{FF}$  from 0 to 1. The pitch angle follows the feedforward update for most of the time, despite of the effect described above. In the time domain some reduction of the generator speed can be observed, but this is more obvious in the frequency domain.

Figure 9b shows the main result of the field testing, which is a reduction of the generator speed variations with the feedforward pitch rate update on, compared to the case with only the feedback controller. However, if the correlation is bad, an increment of the generator speed variations can be seen, because of the wrong pitch action by the feedforward controller in this case.

## 6. Conclusions and Outlook

First results of the field testing show that LIDAR systems can be integrated in current control systems and improve collective pitch control. Although only few data could be collected, the data proofs that it is important to filter the data according to the correlation of the turbine and the LIDAR system. In the case of low correlation, which was due to the impact with the met mast and guy wires, the feedforward controller was not beneficial to the turbine. In the case of high correlation, the standard deviation of the rotor speed has been reduced by 30%.

In further studies, the loads on the turbine will be investigated. In next campaigns the feedback controller should be tuned to focus on the load reduction. Furthermore, the spectra based estimation of the filter will be done online.



**Figure 9.** Results: FFoff(dark gray), good FFon (black), bad FFon (light gray).

### Acknowledgments

Thanks to all persons from NREL and SWE involved in the campaign, especially to the team of Scott Wilde and Lee Fingersh for their help in mounting the LIDAR system and running the turbines, and Jan Anger and Andreas Rettenmeier for their technical support and help in the organization.

NRELs contributions to this report were funded by the Wind and Water Power Program, Office of Energy Efficiency and Renewable Energy of the U.S. Department of Energy under contract No. DE-AC02-05CH11231. The authors are solely responsible for any omission or errors contained herein.

### References

- [1] Harris M, Hand M and Writght A 2006 *Technical Report NREL/TP-500-39154*
- [2] Laks J, Pao L Y, Wright A, Kelley N and Jonkman B 2010 Blade pitch control with preview wind measurements *Proceedings of the 48th AIAA Aerospace Sciences Meeting Including the New Horizons Forum and Aerospace Exposition* (Orlando, USA)
- [3] Dunne F, Schlipf D, Pao L Y, Wright A D, Jonkman B, Kelley N and Simley E 2012 Comparison of two independent lidar-based pitch control designs *Proc. 50th AIAA Aerospace Sciences Meeting Including the New Horizons Forum and Aerospace Exposition*
- [4] Schlipf D, Schlipf D J and Kühn M 2012 *Wind Energy*
- [5] Körber A and King R 2011 Nonlinear model predictive control for wind turbines *Proceedings of the European Wind Energy Association Annual event* (Brussels, Belgium)
- [6] Henriksen L C 2011 *Model Predictive Control of Wind Turbines* Ph.D. thesis Technical University of Denmark
- [7] Kragh K A, Hansen M H and Mikkelsen T 2012 *Wind Energy* ISSN 1099-1824
- [8] Schlipf D, Fischer T, Carcangiu C E, Rossetti M and Bossanyi E 2010 Load analysis of look-ahead collective pitch control using LiDAR *Proceedings of the German Wind Energy Conference DEWEK* (Bremen, Germany)
- [9] Bossanyi E, Wright A and Fleming P 2010 Controller field test on the NREL CART2 turbine Tech. Rep. NREL/TP-5000-49085 NREL
- [10] Rettenmeier A, Bischoff O, Hofsäß M, Schlipf D, Trujillo J J and Kühn M 2010 Wind field analysis using a nacelle-based lidar system *Presentation at the European Wind Energy Conference* (Warsaw, Poland)
- [11] Johnson K, Fingersh L J and Wright A 2005 Controls advanced research turbine: Lessons learned during advanced controls testing Tech. Rep. NREL/TP-500-38130 NREL
- [12] Wright A D, Fleming P and van Wingerden J W 2011 Refinements and tests of an advanced controller to mitigate fatigue loads in the controls advanced research turbine *Proceedings of the 49th AIAA Aerospace Sciences Meeting Including the New Horizons Forum and Aerospace Exposition* (Orlando, USA)
- [13] van der Hooft E and van Engelen T G 2004 *European Wind Energy Conference, London 1 9*
- [14] Buhl M L 2004 WT\_Perf user's guide Tech. Rep. NREL/TP-500-41136 NREL